Image Cover Sheet

CLASSIFICATI:	SYSTEM NUMBER 514689
UNCLASSIFIED	

TITLE

Non-Local Boundary Conditions for High-Order Parabolic Eqyation Algorithms

System Number:

Patron Number:

Requester:

Notes:

DSIS Use only:

Deliver to:

ELSEVIER

Wave Motion 31 (2000) 117–129

WAVE MOTION

www elsevier com/locate/wavemoti

Non-local boundary conditions for high-order parabolic equation algorithms

Gary H. Brooke [a,*], David J. Thomson [b]

[a] *Integrated Performance Decisions, 947 Fort Street, Victoria, BC, Canada V8V 3K3*

[b] *Defence Research Establishment Atlantic, PO 1012, Dartmouth, NS, Canada B2Y 3Z7*

Received 5 March 1999, received in revised form 3 August 1999

Abstract

Numerical parabolic equation (PE) solvers for underwater sound propagation usually approximate the subbottom radiation condition by appending an absorbing layer to the computational mesh An alternative procedure uses a non-local boundary condition (NLBC) applied along (or below) the sea–bottom interface to transform the semi-infinite PE configuration *exactly* into an equivalent bounded domain. In this paper, we analyze NLBCs that are expressed in terms of plane-wave reflection coefficients and describe their implementation in the context of high-order Padé-based PE algorithms In particular, we develop non-local boundary conditions to account for the coherent losses due to scattering by a statistically-rough sea surface Several numerical examples are presented to illustrate the numerical implementation of NLBCs for high-order PEs

1. Introduction

Long range propagation of underwater sound is strongly influenced by interaction with top and bottom ocean boundaries. In deep water, this interaction affects predominantly the high-angle energy and occurs near the ocean surface, e.g., a wind-driven sea surface or the rough underside of multi-year Arctic pack ice. Bottom losses usually limit sea–floor interactions to short ranges in deep water. In contrast, low-frequency sound propagating in shallow water interacts significantly with both boundaries and, consequently, boundary effects are much more prevalent even for low-angle propagation. To complicate matters, the ocean boundaries are often range-dependent and, at some scale, rough. Since popular source localization schemes such as matched field processing [1] rely on correlating acoustic predictions with measured array data, it is important to properly and efficiently model the coherent sound field.

Several numerical models [2,3] are currently used to calculate the transmission of sound underwater — the selection of a particular model depends on the problem at hand. Here, we choose to concentrate on the parabolic equation

* Corresponding author

E-mail address gbrooke@pinc com (G H Brooke)

0165-2125/00/$ – see front matter
PII S0165-2125(99)00039-6

(PE) model since it has application to both shallow and deep water and, in particular, to range-dependent waveguides. PE propagation models have undergone extensive improvements in recent years [3, pp. 343–412]. As attention has shifted to shallow water, the split-step Fourier method [4–6], well-suited to narrow-angle deep-water problems, has been complemented by a suite of finite-difference methods [7–9]. Modern finite-difference PE algorithms have been developed to address specific issues such as accuracy [10–12], energy-conservation [13], and efficiency [14]. Recent models are also capable of treating complicated waveguide effects such as elasticity [15–17], backscatter [18–20] and porosity [21–23]. In this paper we report on two enhancements to finite-difference PE models Specifically, we introduce new non-local boundary conditions (NLBCs) that account approximately for the coherent effects of a rough ocean surface. Combined with previously developed NLBCs that incorporate the interaction of sound with a fluid half-space, we then apply these boundary conditions within the context of high-order Padé [11] and split-step Padé PE [14] algorithms.

A non-local boundary condition for terminating the PE computational grid *exactly* was first introduced to the underwater acoustics community by Papadakis [24, p. 83]. Since then, several workers have derived and implemented NLBCs for modeling one-way wave propagation [25–35]. The derivation of a non-local boundary condition hinges on a priori knowledge of the depth-dependent behavior of the field in a certain portion of the waveguide. For example, if the lowermost half-space is taken to be homogeneous, then the analytic form of the associated field is known and can be accounted for using an impedance boundary condition along the boundary interface. This property still holds in cases where the square of the refractive index in the terminating half-space varies linearly with depth [30,32]. In principle, if the surface impedance function (or equivalently the reflection coefficient) is known as a function of angle, then a non-local boundary condition can be used to account exactly for the effects of any layered inhomogeneous half-space. To date, NLBCs have only been implemented numerically for first-order PE algorithms — the Tappert (Standard) and the Claerbout PEs. Here we extend the application to include high-order Padé and split-step Padé PEs. Furthermore, we utilize the fact that the non-local conditions can be cast in terms of the reflection coefficient to derive approximate NLBCs for a rough zero-mean Gaussian surface. In particular, we demonstrate the application of the modified high-order PE algorithms in an environment where both the rough surface and a penetrable bottom are treated in the context of non-local boundary conditions. We also illustrate the application of NLBCs for a range-dependent waveguide.

2. PE algorithms

Consider a range-independent acoustic medium, bounded above by a free surface at $z = 0$, with a sound speed profile that supports long range propagation (as $r \to \infty$) in the upper part of the waveguide. For $r > 0$, the pressure $p(r, z)$ due to a harmonic point source located at $(r, z) = (0, z_s)$ with time-dependence $\exp(-i\omega t)$ can be obtained by solving the acoustic Helmholtz equation

$$\frac{1}{r}\frac{\partial}{\partial r}\left(r\frac{\partial p}{\partial r}\right) + \rho\frac{\partial}{\partial z}\left(\rho^{-1}\frac{\partial p}{\partial z}\right) + k_0^2 N^2 p = 0. \tag{1}$$

Here k_0 is a reference wavenumber while $\rho(z)$ and $N(z) = n(z)[1 + i\alpha(z)]$ represent the density and the complex refractivity of the stratified medium, respectively. In terms of the reduced field $\psi(r, z) = p(r, z)\sqrt{r}\exp(-ik_0 r)$, the far-field ($k_0 r \gg 1$) form of (1) can be factored to produce an outgoing field component that satisfies the one-way or parabolic equation

$$\frac{\partial \psi}{\partial r} = ik_0\left(-1 + \sqrt{1 + X}\right)\psi, \tag{2}$$

where X is used to denote the differential operator

$$X = N^2 - 1 + k_0^{-2}\rho\frac{\partial}{\partial z}\left(\rho^{-1}\frac{\partial}{\partial z}\right). \tag{3}$$

Using (2), the Taylor expansion $\psi(r+\Delta r,z)=\exp(\partial_r\Delta r)\psi(r,z)$ yields a marching algorithm that forms the basis for all PE methods, i.e.,

$$\psi(r+\Delta r,z)=\exp\left(-\mathrm{i}\delta+\mathrm{i}\delta\sqrt{1+X}\right)\psi(r,z), \tag{4}$$

where we have set $\delta=k_0\Delta r$. There are many numerical approaches for solving (4) that differ only in the treatment used to approximate the square-root operator. Most finite-difference PE methods discretize the waveguide onto an equi-spaced grid of points in depth and range with spacings Δz and Δr, respectively Eq. (4) dictates how the PE field is to be advanced step-by-step in range. Depending on the type, accuracy, and efficiency of PE method desired, specific rational-linear expansions are used to approximate the square-root operator. This procedure exposes the differential operator X in a way that can be handled numerically using a centered-difference representation in the vertical coordinate z (suitably modified to accommodate the density variations)

Basically, two types of Padé expansions are employed in the solution of (4). The first involves a rational-linear or Padé expansion of the square-root operator directly as

$$-1+\sqrt{1+X}\approx\sum_{m=1}^{M}\frac{a_mX}{1+b_mX}. \tag{5}$$

Substituting (5) into (4) leads to a numerical PE solution based on the implicit finite-difference method [3,11], since

$$\psi(r+\Delta r,z)=\prod_{m=1}^{M}\exp\left(\frac{\mathrm{i}\delta a_mX}{1+b_mX}\right)\psi(r,z), \tag{6}$$

can be solved numerically as a sequence of M first-order systems, i.e.,

$$\psi_m(r,z)=\exp\left(\frac{\mathrm{i}\delta a_mX}{1+b_mX}\right)\psi_{m-1}(r,z),\quad m=1,2,\ldots,M, \tag{7}$$

where $\psi_0(r,z)\equiv\psi(r,z)$ and $\psi_M(r,z)\equiv\psi(r+\Delta r,z)$. For $M\geq 2$, the PE algorithm based on (6) is referred to as a high-order Padé PE. For $M=1$, (6) reduces to the Claerbout PE ($a_1=\frac{1}{2}$ and $b_1=\frac{1}{4}$). The Tappert PE is obtained by setting $a_1=\frac{1}{2}$ and $b_1=0$. The Crank–Nicolson procedure for solving each first-order problem in (7) involves approximating the propagator by a unitary rational-linear form to obtain

$$\left(1+c_m^-X\right)\psi_m(r,z)=\left(1+c_m^+X\right)\psi_{m-1}(r,z), \tag{8}$$

where $c_m^{\pm}=b_m\pm\frac{1}{2}\mathrm{i}\delta a_m$. Employing a finite-difference representation of X in (8) yields the familiar tri-diagonal matrix problem for advancing the PE field one range step. If $M=1$, then $\psi_1(r,z)=\psi(r+\Delta r,z)$. For $M>1$, however, $\psi_1(r,z)$ becomes the input for the next first-order problem in the sequence, etc. Typically, for a low-frequency shallow water problem, grid sizes of the order of 5 m in range and 1 m in depth are required in order to accurately propagate the PE field. High-angle propagation is accommodated by taking a larger number of Padé terms.

More recently [14], a second type of Padé expansion has been introduced in the solution of (4) leading to what is known as the split-step Padé PE method In this approach, a Padé expansion is carried out on the exponential propagator itself, i.e.,

$$\exp\left(-\mathrm{i}\delta+\mathrm{i}\delta\sqrt{1+X}\right)\approx 1+\sum_{m=1}^{M}\frac{A_mX}{1+B_mX}. \tag{9}$$

Consequently, (4) becomes

$$\psi(r+\Delta r,z)\approx\psi(r,z)+\sum_{m=1}^{M}\frac{A_mX}{1+B_mX}\psi(r,z). \tag{10}$$

As before, the operator X is handled numerically using finite-differences. Specifically, the solution of (10) is obtained by solving M tri-diagonal problems for the intermediate fields, $\psi_m(r, z)$, derived from

$$(1 + B_m X)\,\psi_m(r, z) = A_m X \psi(r, z), \tag{11}$$

and then by combining the resultant solutions to form

$$\psi(r + \Delta r, z) = \psi(r, z) + \sum_{m=1}^{M} \psi_m(r, z). \tag{12}$$

This procedure advances the PE field one range step. The advantages of the split-step Padé PE over the Padé PE are twofold: (i) the Padé expansion of the propagator allows much larger range steps to be accommodated (by an order of magnitude in some problems), and (ii) the solution of the intermediate problems in (11) involve only the known field at the current range step and can be computed in parallel on a multiple-processor machine.

In obtaining the numerical solution for the intermediate fields, i.e., either (8) or (11), we must truncate the depth grid, top and bottom. In most underwater acoustic applications, the grid is truncated above by a pressure-release ocean surface and below, at a suitably large depth, by a combination of an artificial absorbing layer (to minimize reflections) over a fictitious free boundary. Clearly, the vertical extent of the computational grid is significant in determining the efficiency of the numerical calculations. This fact makes enhancements in range-step capability like that found in the split-step Padé method very attractive. Similarly, procedures that limit the vertical extent of the computational grid are also important, i.e., non-local boundary conditions. Since the PE method is a marching solution, it is routinely applied to range-dependent media by updating the medium at each range step even though it is derived on the basis of range-independence. As will be demonstrated, non-local boundary conditions are applicable to range-dependent problems provided the boundary condition is applied below any range-varying properties in the waveguide.

3. Non-local boundary conditions

Let the ocean/subbottom waveguide combination in $0 < z < z_b$ overlay the uniform fluid half-space $z > z_b$. Traditional finite-difference PE algorithms incorporate boundary conditions associated with this structure by requiring both the pressure $p \propto \psi$ and the vertical particle velocity $v \propto \rho^{-1}\partial_z\psi$ to be continuous across any horizontal interface $z = d \leq z_b$ Because the half-space $z > z_b$ in the present problem is uniform, the PE field in this region must be downgoing in order to satisfy the radiation condition. A non-local boundary condition that represents the field behavior in the lower half-space may be applied along $z = z_b$ to eliminate the need for an absorbing layer and grid terminus combination. In this case, the resultant PE algorithm is unchanged within $0 < z < z_b$, although additional calculations are required to compute the contribution of the non-local boundary condition along $z = z_b$.

In this paper we introduce non-local boundary conditions, applied at $z = 0$ (free surface), to model the coherent losses due to a rough surface with zero-mean Gaussian statistics. Moreover, it is our objective to implement these non-local boundary conditions within the context of a high-order split-step Padé PE algorithm. Up to now, non-local boundary conditions have been used to represent the effects of half-spaces (either homogeneous [27–29] or inhomogeneous [30,32]). These non-local bottom boundary conditions can be combined with NLBCs that treat surface roughness in a single PE code. Previous analyses have been restricted to the first-order Tappert and Claerbout PEs. Since the high-order split-step Padé algorithm involves the definition of intermediate field quantities, we must first establish the boundary conditions satisfied by these fields A modal analysis indicates that the intermediate fields satisfy exactly the same boundary conditions as the total PE field [36]. Thus, for any particular high-order PE, the boundary conditions for the total field can be applied directly to the intermediate fields. It is also important to point out that a NLBC has been derived for (2), which we refer to as the Exact NLBC [28]. To the authors' knowledge,

this NLBC has never been implemented numerically. We include the Exact NLBC in our discussions since it is intimately related to NLBCs for all finite-difference PE algorithms. Finally, we make a distinction between the order (i.e., accuracy) of the NLBC and the order of the PE method used to propagate the acoustic field in the interior of the waveguide. In fact, we demonstrate that low-order NLBCs are quite adequate when used with high-order propagators — a useful result since high-order NLBCs require more complicated numerical implementations.

Our analysis will depend on the Laplace transform pair

$$\Psi(s,z) = \int_0^\infty \psi(r,z)\,\mathrm{e}^{-sr}\,\mathrm{d}r, \quad \psi(r,z) = \frac{1}{2\pi \mathrm{i}}\int_{\varepsilon-\mathrm{i}\infty}^{\varepsilon+\mathrm{i}\infty} \Psi(s,z)\,\mathrm{e}^{+sr}\,\mathrm{d}s, \tag{13}$$

where we assume that the necessary conditions on $\psi(0,z)$ are met such that $\partial_r^l \psi(r,z) \Leftrightarrow s^l \Psi(s,z)$, $l = 1, 2, .$ for $0 \le z \le z_b$. In the transform domain, it is convenient in the derivation of a non-local boundary condition to combine the usual conditions of continuity along $z = d$ into the single continuity condition for the impedance,

$$G(s) \equiv \left.\frac{\rho\Psi}{\partial_z\Psi}\right|_{d-0} = \left.\frac{\rho\Psi}{\partial_z\Psi}\right|_{d+0}. \tag{14}$$

We also utilize a plane-wave analysis in the vicinity of $z = d$ to derive an equivalent form of (14) specified in terms of the plane-wave reflection coefficients, $R^{\pm}(s)$, where the superscript $\pm$ indicates quantities evaluated at $d \pm 0$. Within a thin uniform layer adjacent to $z = d$, we find

$$G(s) = \frac{\rho^{\pm}}{\mp \mathrm{i}\gamma^{\pm}(s)}\frac{1+R^{\pm}(s)}{1-R^{\pm}(s)}, \tag{15}$$

where $\gamma^{\pm}(s)$ is the vertical wavenumber. Rearranging and taking inverse transforms of (14) leads directly to a non-local boundary condition along $z = d$ in the form of a Neumann to Dirichlet (NtD) mapping

$$\psi(r,d) = \int_0^r \partial_z\psi(r-t,d)\underbrace{\frac{1}{2\pi\mathrm{i}}\int_{\varepsilon-\mathrm{i}\infty}^{\varepsilon+\mathrm{i}\infty} G(s)\,\mathrm{e}^{st}\,\mathrm{d}s}_{g(t)}\,\mathrm{d}t\ . \tag{16}$$

Depending on the particular PE approximations involved, the inner integral $g(t)$ can be obtained analytically so that (16) reduces to a single outer integral over the range coordinate t. The ability to carry out this analysis depends on the forms of γ and R for a given problem. In particular, the vertical wavenumber γ is dependent on the specific PE algorithm being implemented and is central to the development of non-local boundary conditions.

3.1. Vertical wavenumbers for PEs

In this section we derive the vertical wavenumbers that can be associated with various PE approximations. The critical equations are (2) for regular Padé PE methods and (4) for split-step Padé PE methods. In the transform domain, (2) for the regular Padé PE becomes

$$s\Psi(s,z) = \mathrm{i}k_0\left(-1+\sqrt{1+X}\right)\Psi(s,z). \tag{17}$$

For the Tappert PE, this equation reduces to

$$s\Psi(s,z) = \frac{1}{2}\mathrm{i}k_0 X\Psi(s,z) \equiv \frac{1}{2}\mathrm{i}k_0\left(N^2(z) - 1 + k_0^{-2}\frac{\partial^2}{\partial z^2}\right)\Psi(s,z), \tag{18}$$

whereupon

$$\left(\frac{\partial^2}{\partial z^2} + \gamma_0^2(s,z)\right)\Psi(s,z) = 0, \tag{19}$$

and γ_0^2 is given in closed form as

$$\gamma_0^2(s,z) = k_0^2\left\{N^2(z) - 1 - 2s/\imath k_0\right\}. \tag{20}$$

The vertical wavenumber for the Exact PE also derives from (17) but involves applying the operator $\imath k_0\sqrt{1+X}$ to both sides and then substituting from (17) to obtain

$$\gamma^2(s,z) = k_0^2\left\{N^2(z) - 1 - (2s/\imath k_0)(1 - \imath s/2k_0)\right\} \equiv \gamma_0^2(s,z) + s^2. \tag{21}$$

With this result, an equivalent expression for the Claerbout PE can be cast in the form

$$\gamma_1^2(s,z) = k_0^2\left\{N^2(z) - 1 - \frac{2s/(\imath k_0)}{1 - s/(2\imath k_0)}\right\} = \gamma^2(s,z) + \mathrm{O}(s^3). \tag{22}$$

The analysis for high-order ($M \geq 2$) Padé PEs is straightforward but more involved. The series obtained by substituting the Taylor expansion

$$-1 + \sqrt{1+X} = \tfrac{1}{2}X - \tfrac{1}{8}X^2 + \tfrac{1}{16}X^3 - \tfrac{5}{128}X^4 + \cdots \tag{23}$$

into (17) can be reverted [37, p. 16] to yield

$$X = 2s/\imath k_0 - s^2/k_0^2 + \mathrm{O}\left(s^{2M+1}\right), \tag{24}$$

from which an expression for the vertical wavenumber associated with the Mth order Padé approximation can be obtained in the form

$$\gamma_M^2(s,z) = \gamma^2(s,z) + \mathrm{O}\left(s^{2M+1}\right). \tag{25}$$

For the split-step Padé PE method, the vertical wavenumbers derive from the transform of (4), i.e.,

$$\exp(s\Delta r)\Psi(s,z) = \exp\left(-\imath\delta + \imath\delta\sqrt{1+X}\right)\Psi(s,z). \tag{26}$$

The series obtained by inserting the Taylor expansions

$$-1 + \exp\left(-\imath\delta + \imath\delta\sqrt{1+X}\right) = \sum_{m=1}^{2M} C_m X^m, \tag{27}$$

$$E(s) = -1 + \exp(s\Delta r) = \sum_{m=1}^{2M} \frac{(s\Delta r)^m}{m!}, \tag{28}$$

where $C_1 = (1/2)\imath\delta$, $C_2 = -(1/8)\delta^2 - (1/8)\imath\delta$, $C_3 = -(1/48)\imath\delta^3 + (1/16)\delta^2 + (1/16)\imath\delta$, etc. into (26) can be reverted for X to yield

$$X = C_1^{-1}E - C_2C_1^{-3}E^2 + \left(2C_2^2 - C_1C_3\right)C_1^{-5}E^3 + \cdots = 2s/\imath k_0 - s^2/k_0^2 + \mathrm{O}\left(s^{2M+1}\right), \tag{29}$$

which results in vertical wavenumbers γ_M of the same order of accuracy in s as those obtained in (25). Apart from the Tappert PE, all of the vertical wavenumbers agree to at least $\mathrm{O}(s^3)$, a somewhat unexpected but useful result.

In principle, with the reflection coefficient R specified, we are in a position to derive non-local boundary conditions for the inhomogeneous waveguide. Unfortunately, only in a few special cases can the inner integral g be carried out analytically. Specifically, these cases involve either the Tappert, the Claerbout, or the Exact vertical wavenumbers — it does not appear possible to proceed analytically when multiple-term regular or split-step Padé approximations

are involved. In order to apply NLBCs to high-order algorithms, we are faced either with performing the inner integral numerically [27,31] or using some alternative approximations. Since γ_M^2 is accurate to second-order in s for $M \geq 1$, we are motivated to go the latter route and use an NLBC derived from a low-order expression for the vertical wavenumber and then apply this boundary condition within the context of a high-order PE algorithm.

3.2. A rough free surface

To derive the non-local boundary condition that represents the effects of a rough zero-mean Gaussian free surface at $z = 0$, we start with the surface reflection coefficient, R_0. In the context of the Claerbout PE, R_0 is given by [3, p. 54]

$$R_0 = -\exp\left[-2\sigma_0^2\gamma_1^2(0)\right], \tag{30}$$

where σ_0 is the rms surface roughness and the explicit dependence on s has been suppressed. Substituting (30) into (15) leads to the surface impedance

$$G_0 = \frac{\mathrm{i}\rho_0}{\gamma_1(0)} \tan h\left[\sigma_0^2\gamma_1^2(0)\right], \tag{31}$$

where $\rho_0 = \rho(0)$. As it stands, G_0 cannot be inverted analytically in (16). For the low-angle energy that is expected to dominate long range propagation, however, a tractable form can be obtained by retaining only the first term in the power series expansion of G_0, i.e.,

$$G_0 = \mathrm{i}\rho_0\sigma_0^2\gamma_1(0) + \mathrm{O}\left(\gamma_1^3\right). \tag{32}$$

Substituting (22) and (32) into (16) and manipulating the inner integrand leads to the approximate non-local rough-surface boundary condition in the form of an NtD map,

$$\begin{aligned}\psi(r,0) - \mathrm{i}k_0\sigma_0^2\sqrt{\kappa_0}\psi_z(r,0) &= \mathrm{i}k_0\sigma_0^2\sqrt{\kappa_0}\int_0^r \psi_z(r-t,0)\left(\frac{1}{2\pi\mathrm{i}}\int_{\varepsilon-\mathrm{i}\infty}^{\varepsilon+\mathrm{i}\infty}\left[\sqrt{\frac{s-2\mathrm{i}k_0\mu_0}{s-2\mathrm{i}k_0}}-1\right]\mathrm{e}^{st}\,\mathrm{d}s\right)\mathrm{d}t \\ &= -k_0\sigma_0^2\sqrt{\kappa_0}\;\tau_0^-\int_0^r \psi_z(r-t,0)\exp(\mathrm{i}\tau_0^+t)\mathcal{K}_+(\tau_0^-t)\,\mathrm{d}t,\end{aligned} \tag{33}$$

where we have defined $\kappa_0 = N_0^2 + 3$, $\kappa_0\mu_0 = N_0^2 - 1$, $\tau_0^{\pm} = k_0(1 \pm \mu_0)$, $N_0 = N(0)$, and introduced the kernel $\mathcal{K}_{\pm}(x) = J_0(x) \pm \mathrm{i}J_1(x)$. J_0, J_1 denote Bessel functions of the first kind. The inverse transform in (33) was evaluated analytically using the result tabulated in [38, p. 60, #561.0].

In contrast, replacing γ_1 with γ_0, a non-local rough-surface boundary condition for the Tappert PE can be derived in the form of the Dirichlet to Neumann (DtN) mapping,

$$\psi_z(r,0) = -\left(B_0/\sigma_0^2\right)\int_0^r \psi(r-t,0)\exp\left(\mathrm{i}b_0t\right)\frac{\mathrm{d}t}{\sqrt{t}}, \tag{34}$$

where $B_0 = \sqrt{\mathrm{i}/(2\pi k_0)}$ and $b_0 = \frac{1}{2}k_0\kappa_0\mu_0$. A similar analysis for the Exact PE determines a non-local rough-surface boundary condition in the DtN form

$$\psi_z(r,0) = -(i/\sigma_0^2)\int_0^r \psi(r-t,0)\exp(-\mathrm{i}k_0t)J_0\left(k_0N_0t\right)\,\mathrm{d}t. \tag{35}$$

The non-local boundary conditions given in (33)–(35) approximate the effects of a rough zero-mean Gaussian free surface at $z = 0$. Because they are based on a low-order series expansion of the vertical wavenumbers for the Claerbout, Tappert and Exact PEs, respectively, they are expected to be most accurate for low-angle propagation

found in shallow-water at long ranges. Each NLBC will be implemented later in the context of the high-order split-step Padé PE algorithm.

3.3. Fluid half-space

For completeness, we include in this section the non-local boundary conditions that represent the effects of a fluid half-space in $z > z_b$ (cf. [27–29]). In this case, the NLBCs account for bottom losses due to the transmission of sound into the sea-bottom. A plane-wave incident upon the interface from $z < z_b$ gives rise to a fluid/fluid reflection coefficient in the form

$$R_b = \frac{\gamma_1(z_b^-) - (\rho_b^-/\rho_b^+)\,\gamma_1(z_b^+)}{\gamma_1(z_b^-) + (\rho_b^-/\rho_b^+)\,\gamma_1(z_b^+)}, \tag{36}$$

where $z_b^\pm = z_b \pm 0$, and $\rho_b^\pm = \rho(z_b^\pm)$. In the Claerbout approximation, substituting (36) into (15) yields the impedance function

$$G_b = \frac{\rho_b^-}{\mathrm{i}\gamma_1(z_b^-)}\frac{1+R_b}{1-R_b} \equiv \frac{\rho_b^+}{\mathrm{i}\gamma_1(z_b^+)}. \tag{37}$$

Use of (37) in conjunction with (16) and (22) leads to an NtD boundary condition for a penetrable sea-bottom in the form (cf. the DtN form given in [28], Eq. (15))

$$\psi(r, z_b) + \frac{\mathrm{i}(\rho_b^+/\rho_b^-)}{k_0\sqrt{\kappa_b}}\psi_z(r, z_b) = -\frac{\tau_b^-(\rho_b^+/\rho_b^-)}{k_0\sqrt{\kappa_b}}\int_0^r \psi_z(r-t, z_b)\exp(\mathrm{i}\tau_b^+ t)\,\mathcal{K}_-(\tau_b^- t)\,\mathrm{d}t, \tag{38}$$

where $\kappa_b = N_b^2 + 3$, $\kappa_b\mu_b = N_b^2 - 1$, $\tau_b^\pm = k_0(1 \pm \mu_b)$, and $N_b = N(z_b^+)$.

Similarly, the NtD condition for the Tappert PE is found to be

$$\psi(r, z_b) = -B_0(\rho_b^+/\rho_b^-)\int_0^r \psi_z(r-t, z_b)\exp(\mathrm{i}b_b t)\,\frac{\mathrm{d}t}{\sqrt{t}}, \tag{39}$$

where $b_b = \frac{1}{2}k_0\kappa_b\mu_b$ while the NLBC corresponding to the Exact PE is

$$\psi(r, z_b) = -\mathrm{i}(\rho_b^+/\rho_b^-)\int_0^r \psi_z(r-t, z_b)\exp(-\mathrm{i}k_0 t)J_0(k_0 N_b t)\,\mathrm{d}t. \tag{40}$$

3.4 Discussion

The Exact NLBCs in (35) and (40) are observed to depend on $J_0(k_0 N t)$ and appear to exhibit improper asymptotic behavior (particularly for lossy media where N is complex). Our derivation of γ in (21) essentially required taking the square of (17) and thus corresponds to the vertical wavenumber associated with the Helmholtz equation As a result, the Exact boundary condition incorporates a component associated with incoming waves, and has the potential for numerical instability when implemented within the context of a one-way algorithm. This aspect of the Exact NLBC will be alluded to in the numerical examples that follow.

In principle, approximate non-local boundary conditions could be derived for high-order Padé and split-step Padé PEs using the same methodology described above, although numerical implementation would prove difficult. Instead, because of the similarity of the vertical wavenumbers (as functions of s) between all PE algorithms, we are motivated to use first-order Tappert and Claerbout NLBCs in conjunction with high-order PE propagators. Our numerical results support this conjecture. Where appropriate (in a lossless waveguide or at a rough free surface) we show that high-order PEs combined with the Exact NLBC can also yield stable and accurate calculations.

4. Numerical examples

An energy-conserving [13] split-step Padé code derived from a finite-difference PE formulation [29,39] has been modified to accommodate each of six different NLBCs described above, i.e., (33)–(35) for the surface roughness and (38)–(40) for the fluid half-space. Three numerical examples are considered that demonstrate specific characteristics or properties of the PE fields generated using the various NLBCs. For the two range-independent test cases, reference solutions were obtained using SAFARI [40], which has the capability of allowing roughness (Gaussian statistics) at interfaces between homogeneous elastic layers [41]. Two-way COUPLE [42,43] is used to provide the reference results for the ASA Wedge problem.

4.1. Example 1: Bucker waveguide

The Bucker waveguide [[3], pp. 249–251] consists of a shallow ocean containing a bilinear sound speed profile $c(z) = 1498 + |120 - z|/60\,\mathrm{m\,s^{-1}}$ and density $1\,\mathrm{g\,cm^{-3}}$ in $0 < z < 240\,\mathrm{m}$ above a uniform fluid of sound speed $1505\,\mathrm{m\,s^{-1}}$ and density $2.1\,\mathrm{g\,cm^{-3}}$, respectively There is no intrinsic loss in this problem. Calculations are carried out at a frequency of 100 Hz for a source depth of 30 m and a receiver depth of 90 m. SAFARI and split-step Padé PE transmission losses $(-10\log_{10}|p|^2)$ versus range are compared in Fig 1. The PE curve was obtained using $M = 2$, $\Delta r = 10\,\mathrm{m}$, $\Delta z = 1\,\mathrm{m}$ with the Claerbout (C) NLBC applied along $z = 240\,\mathrm{m}$. The agreement is seen to be excellent. Corresponding results obtained with the Tappert (T) NLBC using $M = 2$, $\Delta r = 100\,\mathrm{m}$ and the Exact (E) NLBC using $M = 3$, $\Delta r = 400\,\mathrm{m}$ are compared to the SAFARI curve in Fig. 2. Although the range sampling is too large to resolve individual peaks at shorter ranges, the agreement at longer ranges is excellent. The Bucker problem demonstrates, in principle, that the use of NLBCs does not compromise the efficiency of the split-step Padé algorithm, i.e , the ability to take large range steps. Although the Bucker problem is relatively benign in the sense that it involves narrow-angle propagation, it does show that each of the fluid half-space NLBCs can be incorporated within the context of a multi-term split-step Padé PE.

4.2. Example 2: Pekeris waveguide

Example 2 corresponds to the Pekeris waveguide introduced at a NORDA Workshop as test case 3 [24]. The region $0 < z < 100\,\mathrm{m}$ contains a homogeneous fluid with sound speed $1500\,\mathrm{m\,s^{-1}}$ and density $1\,\mathrm{g\,cm^{-3}}$ that overlays a fluid half-space with constant sound speed, density and absorption of $1590\,\mathrm{m\,s^{-1}}$, $1.2\,\mathrm{g\,cm^{-3}}$ and 0 5

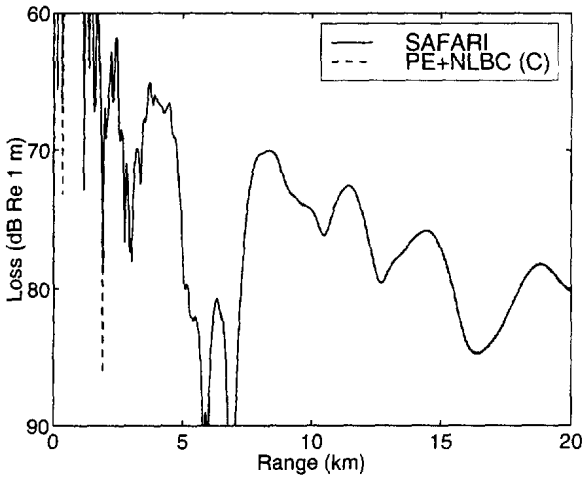

Fig 1 Transmission loss comparison for the Bucker waveguide

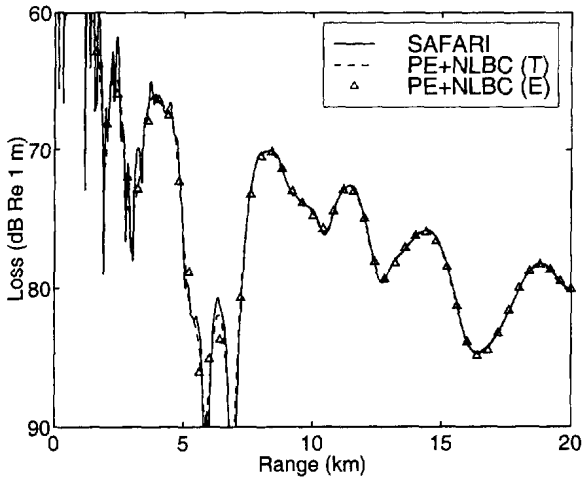

Fig 2 Transmission loss comparison for the Bucker waveguide

dB λ^{-1}, respectively. The source and receiver depths are both equal to 50 m. The 250 Hz source frequency gives rise to 11 propagating modes in this waveguide. In addition to the original waveguide configuration, we consider a modified version obtained by adding an rms surface roughness of 4 m.

The SAFARI and PE transmission loss results shown in Fig. 3 compare the propagation for a smooth surface ($\sigma_0 = 0$ m) to that of a rough surface ($\sigma_0 = 4$ m) for the Pekeris waveguide. For the PE calculations, we used a two-term Padé approximation ($M = 2$) and grid sizes $\Delta r = 5$ m, $\Delta z = 0.25$ m. The PE results for $\sigma_0 = 0$ were obtained by applying Claerbout's (C) NLBC along $z = 100$ m. In contrast, the PE results for $\sigma_0 = 4$ m were obtained using NLBCs applied along both $z = 0$ and $z = 100$ m. At this frequency, the 4 m rms surface roughness is observed to have a considerable effect on the far-field propagation. Due to the stripping of the high-order modes, the transmission loss results are considerably smoother and the overall levels have increased by several dB. Similar agreement (not shown) is obtained with the Tappert NLBC.

Further PE calculations for this example, also not shown here, were carried out using $M = 3$, $\Delta r = 50$ m. Although stable, the results obtained with Tappert's NLBC applied top and bottom for this larger range step size are

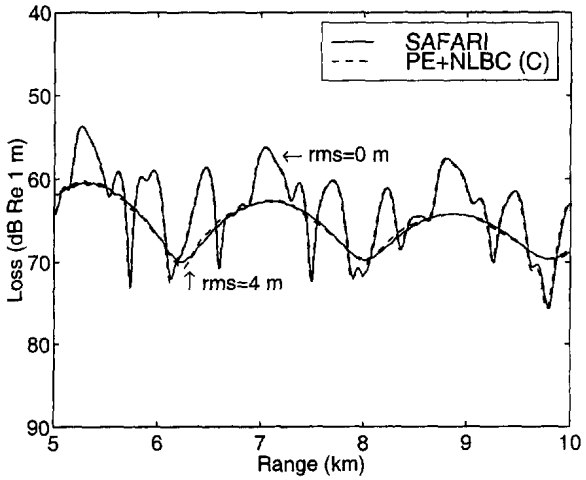

Fig 3 Transmission loss comparison for the Pekeris waveguide

not as good as those shown in Fig. 3 and indicate a limitation on Δr for this problem. On the other hand, the Exact NLBC applied along $z = 100$ m was found to be unstable in this case for either value of Δr. We believe that this is due to the presence of loss in the lower half-space and the improper asymptotic behavior of $J_0(k_0 N t)$ Moreover, the agreement obtained for the Claerbout NLBC using $M = 3$, $\Delta r = 50$ m is considerably worse than that for the Tappert NLBC. We attribute this decrease in accuracy to approximations inherent in our numerical integration procedure for integrals involving Bessel functions. Unfortunately, for this problem, our current numerical scheme [36] for implementing this boundary condition precludes the capability for larger step sizes that are characteristic of split-step Padé methods.

4.3. Example 3: ASA wedge

The ASA wedge [43] is a shallow-water shoaling waveguide in which the water depth decreases from 200 m to 0 over a range of 4 km. The homogeneous wedge has a sound speed of 1500 m s^{-1} and a density of 1 g cm^{-3}. The fluid bottom has a constant sound speed, density and absorption of 1700 m s^{-1}, 1.5 g cm^{-3} and 0.5 dB λ^{-1}, respectively. Calculations are carried out at 25 Hz for a source located at $r = 0$ km and $z = 100$ m. For this range-dependent problem, the non-local boundary conditions in (38)–(40) were applied at a depth of 202 m, just below the water/bottom interface at the range of the source and below any changes in material properties of the medium. Consequently, the NLBCs act solely to absorb downgoing energy in this problem. Curves of transmission loss versus range calculated for a receiver at a depth of 30 m are shown in Fig. 4 The reference results were obtained using the coupled mode code COUPLE [42,43]. The energy-conserving PE curve for the Claerbout (C) NLBC, calculated using $\Delta r = 5$ m, $\Delta z = 1$ m, $M = 2$, agrees well with the COUPLE curve. PE results obtained using $M = 3$, $\Delta r = 50$ m for the Exact (E) and Tappert (T) non-local boundary conditions (not shown) depart slightly from the good agreement shown in Fig. 4. For this larger range step size, the observed departures from the coupled mode results are due to the range-dependence of the sloping interface and not to the numerical approximations used in evaluating the NLBCs, despite the fact that the bottom half-space is lossy. Evidently, at the low-frequency and short ranges considered for this problem, the potential difficulties with computing Bessel functions of complex arguments is not an issue. This test case demonstrates that the NLBCs can be applied to range-dependent problems in a straightforward and efficient manner.

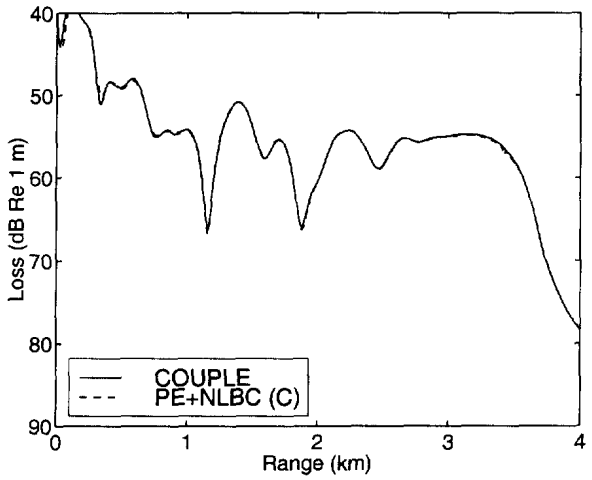

Fig 4 Transmission loss comparison for the ASA wedge

5. Summary

An analysis of non-local boundary conditions applied in the context of multi-term high-order PE algorithms has been carried out. Specifically, it has been verified numerically that NLBCs derived on the basis of the boundary conditions satisfied by the total field also apply to the individual intermediate fields associated with high-order solution procedures. High-order PEs can be combined with a formulation of the impedance boundary condition, based on the plane-wave reflection coefficient, to obtain non-local boundary conditions representing a wide range of waveguide layering and scattering effects. It has also been shown that the vertical wavenumber $\gamma_M(s)$ associated with an Mth order PE field provides a useful framework for analyzing non-local boundary conditions. Since γ_M agrees with γ for the Exact PE to O $\left(s^{2M+1}\right)$, low-order PE approximations lead to vertical wavenumbers that approximate those corresponding to high-order algorithms. Consequently, high-order NLBCs, which are difficult to implement numerically, can be replaced by non-local boundary conditions based on low-order PE approximations and then used in conjunction with the high-order propagators interior to the computational domain. For the special case of a rough surface characterized by Gaussian statistics, we imposed a low-angle condition to derive an approximate NLBC that can be easily implemented in high-order PEs. Three examples involving rough sea surfaces and/or penetrable ocean bottoms were used to demonstrate the implementation of non-local conditions in a multi-term, split-step Padé PE. For most examples, the NLBCs did not degrade the large range step capability of the split-step Padé algorithm.

References

[1] A Tolstoy, Matched Field Processing in Underwater Acoustics, World Scientific, Singapore, 1993
[2] M J Buckingham, Ocean-acoustic propagation models, J Acoustique 3 (1992) 223–287
[3] F B Jensen, W A Kuperman, M B Porter, H Schmidt, Computational Ocean Acoustics, American Institute of Physics, New York, 1994
[4] F D Tappert, R H Hardin, Computer simulation of long-range ocean acoustic propagation using the parabolic equation method, in Proceedings of the Eighth International Congress on Acoustics, vol 2, Goldcrest, London, 1974, p 452
[5] F D Tappert, The parabolic approximation method, in J B Keller, J S Papadakis (Eds), Wave Propagation and Underwater Acoustics, Springer, New York, 1977, pp 224–287
[6] D J Thomson, N R Chapman, A wide-angle split-step algorithm for the parabolic equation, J Acoust Soc Amer 74 (1983) 1848–1854
[7] D Lee, S.T McDaniel, Ocean acoustic propagation by finite-difference methods, Comput Math Appl 14 (1987) 305–423
[8] M D Collins, Higher-order, energy-conserving, two-way, and elastic parabolic equations, in S A Chin-Bing, D B King, J A Davis, R B Evans (Eds), PE Workshop II Proceedings of the Second Parabolic Equation Workshop, US Government Printing Office, Washington, DC, 1993, pp 145–168
[9] M D Collins, R J Cederberg, D B King, S A Chin-Bing, Comparison of algorithms for solving parabolic wave equations, J Acoust Soc Amer 100 (1996) 178–182
[10] A Bamberger, B Engquist, L Halpern, P Joly, Higher order paraxial wave equation approximations in heterogeneous media, SIAM J Appl Math 48 (1988) 129–154
[11] M D Collins, Benchmark calculations for higher-order parabolic equations, J Acoust Soc Amer 87 (1990) 1535–1538
[12] F A Milinazzo, C A Zala, G H Brooke, Rational square-root approximations for parabolic equation algorithms, J Acoust Soc Amer 101 (1997) 760–766
[13] M D Collins, E K Westwood, A higher-order energy-conserving parabolic equation for range-dependent ocean depth, sound speed, and density, J Acoust Soc Amer 89 (1991) 1068–1075
[14] M D Collins, The split-step Padé solution for the parabolic equation method, J Acoust Soc Amer 93 (1993) 1736–1742
[15] M D Collins, A higher-order parabolic equation for wave propagation in an ocean overlying an elastic bottom, J Acoust Soc Amer 86 (1989) 1459–1464
[16] B T R Wetton, G H Brooke, One-way wave equations for seismoacoustic propagation in elastic waveguides, J Acoust Soc Amer 87 (1990) 624–632
[17] M D Collins, Higher-Order Padé approximations for accurate and stable elastic parabolic equations with application to interface wave propagation, J Acoust Soc Amer 89 (1991) 1050–1057
[18] M D Collins, R B Evans, A two-way parabolic equation for acoustic backscattering in the ocean, J Acoust Soc Amer. 91 (1992) 1357–1368
[19] G H Brooke, D J Thomson, A single-scatter formalism for improving PE calculations in range-dependent media, in S A Chin-Bing, D B King, J A Davis, R B Evans (Eds), PE Workshop II Proceedings of the Second Parabolic Equation Workshop, US Government Printing Office, Washington, DC, 1993, pp. 126–144

[20] M D Collins, A two-way parabolic equation for elastic media, J Acoust Soc Amer 93 (1993) 1815–1825
[21] M D Collins, W A Kuperman, W L Siegmann, A parabolic equation for poro-elastic media, J Acoust Soc Amer 98 (1995) 1645–1656
[22] M D Collins, J F Lingevitch, W L Siegmann, Wave propagation in poro-acoustic media, Wave Motion 25 (1997) 265–272
[23] J F Lingevitch, M D Collins, Wave propagation in range-dependent poro-acoustic waveguides, J Acoust Soc Amer 104 (1998) 783–790
[24] J A Davis, D White, R C Cavanagh, NORDA Parabolic Equation Workshop, 31 March to 3 April 1981, Tech Note 143, Naval Ocean Research and Development Activity, NSTL Station, Mississippi, 1982
[25] S W Marcus, A generalized impedance method for application of the parabolic approximation to underwater acoustics, J Acoust Soc Amer 90 (1991) 391–398
[26] V A Baskakov, A V Popov, Implementation of transparent boundaries for numerical solution of the Schrodinger equation, Wave Motion 14 (1991) 121–128
[27] J S Papadakis, M I Taroudakis, P J Papadakis, B Mayfield, A new method for a realistic treatment of the sea bottom in the parabolic approximation, J Acoust Soc Amer 92 (1992) 2030–2038
[28] J S Papadakis, Exact, nonreflecting boundary conditions for parabolic-type approximations in underwater acoustics, J Comput Acoust 2 (1994) 83–98
[29] D J Thomson, M E Mayfield, An exact radiation condition for use with the a posteriori PE method, J Comput Acoust 2 (1994) 113–132
[30] T W Dawson, D J Thomson, G H Brooke, Non-local boundary conditions for acoustic PE predictions involving inhomogeneous layers, in J S Papadakis (Ed), Third European Conference on Underwater Acoustics, FORTH-IACM, Heraklion, 1996, pp 183–188
[31] M E Mayfield, D J Thomson, An FFT-based non-local boundary condition for the parabolic equation, in J S Papadakis (Ed), Third European Conference on Underwater Acoustics, FORTH-IACM, Heraklion, 1996, pp 237–242
[32] M F Levy, Transparent boundary conditions for parabolic equation solutions of radiowave propagation problems, IEEE Trans Antennas and Propagation 45 (1997) 66–72
[33] D J Thomson, G H Brooke, Non-local boundary conditions for 1-way wave propagation, in J A DeSanto (Ed), Fourth International Conference on Mathematical and Numerical Aspects of Wave Propagation, SIAM, Golden, 1998, pp 348–352
[34] A Arnold, M Ehrhardt, Discrete transparent boundary conditions for wide angle parabolic equations in underwater acoustics, J Comput Phys 145 (1998) 611–638
[35] D Yevick, D J Thomson, Nonlocal boundary conditions for finite-difference parabolic equation solvers, J Acoust Soc Amer 106 (1999) 143–150
[36] G H Brooke, D J Thomson, Non-local boundary conditions for high-order PE models with application to scattering from a rough surface, Technical Memorandum DREA TM 1999-121, Defence Research Establishment Atlantic, Dartmouth, N S , 1999
[37] M Abramowitz, A Stegun, Handbook of Mathematical Functions, Dover, New York, 1965
[38] G A Campbell, R M Foster, Fourier Integrals for Practical Applications, Van Nostrand, New York, 1948
[39] D J Thomson, Wide-angle parabolic equation solutions to two range-dependent benchmark problems, J Acoust Soc Amer 87 (1990) 1514–1520.
[40] H Schmidt, SAFARI Seismo-Acoustic Fast Field Algorithm for Range-Independent Environments User's Guide, Report SR-113, SACLANTCEN ASW Research Centre, San Bartolomeo, Italy, 1988
[41] W A Kuperman, H Schmidt, Rough surface elastic wave scattering in a horizontally stratified ocean, J Acoust Soc Amer 79 (1986) 1767–1777.
[42] R B Evans, A coupled mode solution for acoustic propagation in a waveguide with stepwise depth variations of a penetrable bottom, J Acoust Soc Amer 74 (1983) 188–195
[43] F B Jensen, C M Ferla, Numerical solution of range-dependent benchmark problems in ocean acoustics, J Acoust Soc Amer 87 (1990) 1499–1510

#514689